THE UNIVERSITY of EDINBURGH

Edinburgh Research Explorer

Microstructure-based equivalent visco-hyperelastic model of viscoelastic damper

Citation for published version:
Li, Q, Xu, ZD, Dong, Y-R, He, Z-H, He, J & Lu, Y 2022, 'Microstructure-based equivalent visco-hyperelastic model of viscoelastic damper', *Journal of Engineering Mechanics*, vol. 148, no. 4, 04022014, pp. 1-15. https://doi.org/10.1061/(ASCE)EM.1943-7889.0002092

Digital Object Identifier (DOI):
10.1061/(ASCE)EM.1943-7889.0002092

Link:
Link to publication record in Edinburgh Research Explorer

Document Version:
Peer reviewed version

Published In:
Journal of Engineering Mechanics

General rights
Copyright for the publications made accessible via the Edinburgh Research Explorer is retained by the author(s) and / or other copyright owners and it is a condition of accessing these publications that users recognise and abide by the legal requirements associated with these rights.

Take down policy
The University of Edinburgh has made every reasonable effort to ensure that Edinburgh Research Explorer content complies with UK legislation. If you believe that the public display of this file breaches copyright please contact openaccess@ed.ac.uk providing details, and we will remove access to the work immediately and investigate your claim.

OPEN ACCESS

Download date: 25. Apr. 2022

Microstructure-based equivalent visco-hyperelastic model of viscoelastic damper

Qiang-Qiang Li[1], Zhao-Dong Xu, A. M. ASCE[2*], Yao-Rong Dong[3], Zhen-Hua He[4], Jia-Xuan He[5], Yong Lu, F. ASCE [6]

Abstract: Mechanical properties of viscoelastic (VE) dampers directly affect the aseismic performance of viscoelastically damped structures, it is of great significance to accurately describe the nonlinear mechanical characteristics of VE dampers in the aseismic design and analysis of structures. However, most of the existing mathematical models for VE dampers have been established from a macroscopic perspective, and there is a general lack of a comprehensive connection to the microstructure characteristics of VE materials and external influence factors such as loading frequency, ambient temperature, and strain amplitude. In this paper, inspired by the molecular chain network models and fractional derivative theory, a microstructure-based equivalent visco-hyperelastic model is proposed for VE dampers with consideration of the temperature dependence and the filler reinforcement effect. To verify the characterization capacity of the proposed model, laboratory

1 Ph.D. Candidate, Key Laboratory of C&PC Structures of the Ministry of Education, Southeast University, Nanjing 210096, China. E-mail: LI_QiangQiang2018@163.com

2 Professor, Key Laboratory of C&PC Structures of the Ministry of Education, Southeast University, Nanjing 210096, China. (Corresponding author) E-mail: zhdxu@163.com

3 Associate Professor, School of Civil Engineering, Xi'an University of Architecture and Technology, Xi'an 710055, China; Key Lab of Structural Engineering and Earthquake Resistance, Ministry of Education (XAUAT), Xi'an 710055, China;

4 Ph.D. Candidate, School of Civil Engineering, Xi'an University of Architecture and Technology, Xi'an, China. E-mail: HeZhenHua_DY@163.com

5 Ph.D. Candidate, Key Laboratory of C&PC Structures of the Ministry of Education, Southeast University, Nanjing 210096, China. E-mail: jxhe@seu.edu.cn

6 Professor, Institute for Infrastructure and Environment, School of Engineering, The University of Edinburgh, UK. E-mail: Yong.Lu@ed.ac.uk

experiments on the dynamic property of VE dampers were carried out with varying frequencies, temperatures, and strain amplitudes, the proposed model is then employed to predict the experimental results. Finally, the model parameter analysis is conducted to clarify the relationship between material microstructure and its macroscopic performance. The experiments indicate that the VE damper possesses an excellent energy dissipation capability, and characteristic parameters of VE dampers tend to be more sensitive in the low ranges of frequency and temperature than that in the high ranges. Comparisons between the experimental and numerical results suggest that the proposed model can describe the mechanical properties of VE dampers at different frequencies, temperatures, and strain amplitudes with good accuracy. Parameter analysis demonstrates that the proposed model can reflect the influence of material microstructure on the macroscopic mechanical properties of VE damper.

Keywords: viscoelastic damper; microstructure of viscoelastic material; dynamic property tests; mathematical model; parameter analysis.

Introduction

VE dampers have been widely used in building structures for mitigating vibrations from earthquake. The vibration mitigation effects of VE dampers have typically been studied at the device level through experiments and simulations. Chang et al. (1992) tested the dynamic performance of VE dampers under different frequencies and temperatures. To study the temperature and frequency dependence of VE dampers and the phenomenon of self-heating in the working process, Kasai (2001) conducted a series of experiments on the mechanical properties of VE dampers. Xu et al. (2020) tested the dynamic

mechanical properties of Acryl-rubber VE dampers. Min et al. (2004) and Chang and Lin (2004) experimentally demonstrated that the installation of VE dampers significantly enhanced the overall aseismic performance of structures. Dong et al. (2020) found that VE haunch bracing-damper can observably upgrade the seismic performance of RC frames.

On the other hand, the VE dampers are well recognized to exhibit complex nonlinear mechanical behaviors under dynamic loads. As the main energy-dissipation component in the damping system, it is important to establish a sound theoretical model to describe the mechanical properties of the VE dampers so as to guide their continued development. Classical rheological models are capable of describing the dynamic properties of VE dampers by combining different numbers of spring elements and Newton pots (Zhou et al. 2016). Considering that VE dampers exhibit different kinds of non-standard gradient rates, the fractional differential operators, which can well reflect this phenomenon in a wide frequency domain, have been incorporated, and some rheological fractional derivative models are then developed, such as fractional Kelvin model, fractional Zener model, and generalized fractional derivative model (Lewandowski and Przychodzki 2018; Li et al. 2021; Xu et al. 2013). However, these models are all macroscopic phenomenological models, the model parameters generally lack clear physical meaning, and there is no direct connection among the macroscopic mechanical properties and damping mechanism of VE dampers and the microstructure of VE material.

To demonstrate the underlying mechanical behavior of VE dampers more clearly, some mathematical models based on the multi-scale method have been developed. Li et al. (2012) proposed a multi-scale calculation strategy to describe the dynamic mechanical properties of VE materials. Tomita et al. (2006) presented a constitutive model with the consideration of the interactions between the molecular chains of the carbon black-filled rubber based on the assumption of homogeneity. To facilitate engineering

applications of multi-scale models, Kroon (2011) and Xu et al. (2016) presented microscopic chain models by combining the molecular chain models and rheological models. Xu et al. (2019) proposed a polyhedral network chain model based on the statistical theory of molecular dynamics. The aforementioned studies indicate that the microstructure of VE material can greatly affect the mechanical properties of VE dampers, thus it is beneficial for the development of VE dampers to study the mechanical behaviors of VE materials from a microscopic standing point of view. However, most of existing microscopic models are only based on assumptions of specific behaviors of VE materials and are not capable of comprehensively considering the effects of the material microstructure, such as geometric entanglement of molecular chain, statistical difference of molecular chain configurations, filler-rubber matrix structure, as well as external factors that influence the material behaviors, including temperature, loading frequency, and strain amplitude.

In the present paper, a microstructure-based mathematical model for describing the mechanical properties of VE dampers is developed with consideration of its temperature-, frequency-, and strain-dependence. This model is based on the macroscopic rheological models and molecular chain models from the microscopic perspective, so that it is capable of fully reflecting the relationship between the microscopic characteristics of VE material and the macroscopic mechanical behaviors of VE dampers with clear physical meanings under varying temperature, frequency, and strain conditions. In conjunction with the above model development, laboratory experiment on the dynamic properties of the VE dampers have also been conducted, and the accuracy and applicability of the proposed model are verified by the test data, based on which the parameter analysis are finally carried out. The results indicate that the microstructure-based equivalent visco-hyperelastic model can accurately represent the mechanical properties of VE dampers in a physically meaningful manner.

Microstructure-based equivalent visco-hyperelastic model

VE material usually needs to be vulcanized to enhance its mechanical properties. In the vulcanization process with high temperature and high pressure, elastic network chains and free chains can form inside the VE material. The elastic network chain is closely related to the elastic properties of the VE material, and the free network chain, which includes uncrosslinked chain and side chain without network structure, on the other hand, is the primary source of the viscosity for the energy dissipation of the matrix rubber (Miehe and Göktepe 2005; Tang et al. 2012). Under dynamic loads, VE material simultaneously shows the hyperelastic characteristics, including large elongation and recoverable deformation, and the viscosity characteristics, such as rate dependence, loading history memory, and relaxation. For the above reasons, most mathematic models describing the constitutive behaviors of VE materials are formulated from consideration of these two aspects (Boccaccio et al. 2015; Shim et al. 2010; Xu et al. 2016; Xu et al. 2019; Xu et al. 2019; Yang et al. 2000).

However, it should be pointed out that the elastic network chains and free chains usually do not exist alone, and each contributes to the elasticity and viscosity of materials simultaneously. Besides, these two types of molecular chains always interlace with each other and form a very complicated geometric topological network structure. With the influence of filler structures, a single molecular chain is often significantly constrained by surrounding molecular chains, thus the VE material gets strengthened. Figure 1 shows the actual microstructure of the VE material obtained by using the scanning electron microscope (SEM) technology and its simplified model of the molecular chain topological structure. However, this effect is barely considered in the common microscopic chain models (Boyce and Arruda 2000; Marckmann et al. 2002; Treloar 1946; Treloar and Riding 1979).

To reflect the influence of material microstructure on its macroscopic mechanical properties, the stress of VE material, σ, is divided into three parts, namely hyperelastic stress σ_s, viscous stress σ_v, and constraint stress σ_c, as:

$$\sigma = \sigma_s + \sigma_v + \sigma_c \tag{1}$$

where σ_s and σ_v represent the contributions of network chain and free chain to the elasticity and viscosity of VE material, respectively; σ_c introduced here, in particular, is utilized to account for the influences of constraints from surrounding molecular chain network on the elasticity and viscosity of VE material. The following section will focus on the derivation of the three stresses and the establishment of the mathematical model for VE dampers used in structural earthquake resistance.

Statistical evolution model for characterizing the hyperelasticity behavior

Assuming that the end-to-end distance between each crosslinking point of the molecular chain network conforms to the Gaussian distribution, Treloar (1946) proposed the Gauss model to describe the mechanical behavior of elastomer, as:

$$W_G = \frac{1}{2} N_1 k T_0 \sum_{j=1}^{3} \left(\lambda_j^2 - 1\right) \tag{2}$$

where N_1 is the number of elastic chains per unit volume, k is the Boltzmann constant, T_0 is the absolute temperature, $\lambda_j (j = 1,2,3)$ is the principal elongation in three directions, W_G is the Gaussian stitastics based strain energy in the isothermal condition. Hereinafter, in the derivation of other strain energies, it naturally assumed that the VE damper is in an isothermal condition, and there is no heat exchange with the outside for the whole system.

The stress-strain relationship of VE material can be obtained by:

$$\sigma_j = \frac{\partial W}{\partial \lambda_j} \lambda_j - P \tag{3}$$

where σ_j is the principal stress in the direction of principal elongation, W is the strain energy of VE material, P is the hydrostatic pressure calculation based on boundary conditions.

For the shear-deformation mode, based on Equation (2) and (3), the stress described by the Gauss model can be determined by ignoring the hydrostatic pressure, as:

$$\sigma_G = N_1 k T_0 (\lambda^2 - \lambda^{-2}) \tag{4}$$

Replacing λ by the engineering strain ε in Equation (4), and applying the Taylor expansion on the polynomial of ε, the corresponding shear stress σ_G can be obtained by omitting the higher-order term of ε:

$$\sigma_G = 4 N_1 k T_0 \varepsilon \tag{5}$$

However, the radial distribution of the end-to-end distance for the molecular chains may no longer conform to the Gaussian distribution once the end distance reaches 40% of the total elongation (Boyce and Arruda 2000; Marrucci 1988), and some non-Gaussian models are then introduced. Among them, the latest and most widely used is the 8-chain model based on Langevin's statistical theory (Boyce and Arruda 2000). For simplification in the actual application, the Maxwell element is incorporated here to describe the entropy-elastic characteristics of each chain segment in the 8-chain model, of which the force-displacement relationship can be expressed as:

$$F_{8ch} = \frac{pq\omega^2 + q\omega i}{1 + p^2\omega^2}(r - r_0) = E_{8ch}(r - r_0) \tag{6}$$

where F_{8ch} is the corresponding force at the end of molecular segment force under deformation, E_{8ch} is the corresponding equivalen stiffness of a single chain, p and q are material parameters, ω is the loading frequency, i is the imaginary unit, r_0 and r are the end-to-end distances of molecular chains before and after deformation, respectively, which are employed here to represente the relative

deformation at both ends of molecular chain. The strain energy of a single molecular chain in the 8-chain model after deformation w_{8ch} is then obtained, as:

$$w_{8ch} = \frac{1}{2} E_{8ch}(r - r_0)^2 \tag{7}$$

Considering that the volume of cube represented by the 8-chain network is $\frac{8\sqrt{3}}{9} r_0^3$, based on Equation (7), the total energy of a single molecular chain per unit volume for the Maxwell 8-chain model W_{8ch} is expressed as:

$$W_{8ch} = N_1 \frac{3\sqrt{3}}{2r_0^3} \cdot \frac{1}{8} w_{8ch} \tag{8}$$

Assuming the deformation mode of molecular chain conforms to the affine deformation, the displacement of a single molecular chain during deformation can be described as $|r - r_0|^2 = [(\lambda_1 - 1)^2 + (\lambda_2 - 1)^2 + (\lambda_3 - 1)^2] r_0^2$.

Substituting Equation (8) into (3) yields the non-Gaussian-based shear stress σ_{8ch}, as:

$$\sigma_{8ch} = \frac{3\sqrt{3} N_1}{4r_0} \frac{pq\omega^2 + q\omega i}{1 + p^2\omega^2} \varepsilon \tag{9}$$

Comparing to the Gauss model, the 8-chain model can well reflect the influence of ultimate elongation on the conformation of the molecular chain network in large deformation, but it becomes deficient in the small deformation stage (Boyce and Arruda 2000; Wu and Van Der Giessen 1993). To solve this problem, some hybrid models based on different statistical methods are developed to approximate the radial distribution characteristics of material molecular chains. Boyce and Arruda (2000) and Wu and Van Der Giessen (1993) proposed mixed models to characterize the elastic behavior of polymer based on the linear superposition of two different non-Gaussian models, and found that the predictive performance of mixed models are much better than the single two models. However, a single chain

distribution assumption is not in line with reality from a statistical point of view. Elías-Zúñiga and Beatty (2002) proposed a composite model through the linear superposition of an amended 3-chain model and amended 8-chain model, in which these two sub-models can reduce to the Gaussian model. Lim (2005) introduced a nonlinear evolution function and presented a hybrid model by combining a Gaussian model and a non-Gaussian model.

In fact, the configuration distribution of molecular chains in the VE material is variable with the change of deformation state. The two ideal extremes of distribution evolution for molecular chains are the complete Gaussian distribution at small deformation and the complete non-Gaussian distribution at large deformation, respectively, and there exists a critical deformation to distinguish these two states beyond which the non-Gaussian model should prevail (Lim 2005), which can be visualized as Figure 2.

This means the constructed statistical evolution function should be able to smoothly transform between two different distributions according to the strain state. Based on this, considering that a single chain distribution assumption is not in line with reality from a statistical point of view, a linear combination of the Gaussian chain and 8-chain models in accordance with the simple mixture rule is dopted in the present study to express the hyperelasticity of VE material, as:

$$\sigma_s = \xi\sigma_{8ch} + (1-\xi)\sigma_G \tag{10}$$

where ξ is a transition function introduced herein to describe the evolution of chains statistic distribution under different strain states. It can be seen that the selection of transition equation ξ is very important in the establishment of specific mixed distribution model. Considering the above description, when the displacement exceeds ε_{tr}, the non-Gaussian distribution should dominate, while the

Gaussian distribution should dominate when ε_{tr} is not exceeded. Therefore, transition function ξ in Equation (10) should satisfy the following conditions:

$$\begin{cases} \xi \longrightarrow 0 & \varepsilon < \varepsilon_{tr} \\ \xi \longrightarrow 1 & \varepsilon > \varepsilon_{tr} \end{cases} \tag{11}$$

where ε is the actual deformation state, and the arrow means approaching. In the specific construction of ξ, different forms of transition equation have been proposed in previous studies (Elías-Zúñiga and Beatty 2002; Lim 2005), and a comparison with the present proposal with $\varepsilon_{tr} = 0.1$, respectively, as shown in Figure 3.

It can be seen that the transition equation shown in Figure 3(a) and (c) do not show a gradual trend at both ends, but shows a monotonous increase or decrease, which seriously deviate from the requirements of Equation (2) within the common strech range of 0~5 for VE material. Based on these, herein we introduct an new transition function by incorporating the generalized logic function, as:

$$\xi = \frac{1}{(1 + e^{\varepsilon_{tr} - \varepsilon})^5} \tag{12}$$

The order of the generalized logic function is determined as 5 by satisfying the function range for ξ, that is, satisfying Equation (11), with the corresponding transition equation curve shown in Figure 3(b). As observed, this S-type curve can describe the evolution of two statistical distributions of molecular chains under different deformation states in a smooth manner, which is more reasonable than the other two. In practice, the determination of ε_{tr} is complex and difficult to be carried out through direct tests. Therefore, we use the method of fitting the test data to obtain ε_{tr}, which is also a common practice at present.

The fractional derivative 3-chain model for Characterizing the viscosity property

VE material exhibits the mechanical properties between the ideal solid and Newtonian fluid, and the fractional differential theory has been proved to be suitable for describing this abnormal physical phenomenon. For this reason, Lewandowski and Pawlak (2011) introduced the Abel fractional element to describe the behaviors of VE material, the constitutive relation of which is expressed as:

$$\sigma_v = \zeta D^{\gamma} \varepsilon(t) \tag{13}$$

where ζ is the viscosity of VE materials, $\varepsilon(t)$ represents the time-dependent strain function, and D^{γ} is the fractional derivative operator, γ is the order of the derivative.

However, these existing fractional derivative models are all macroscopic mathematical models and they do not explain the underlying microstructure processes. Therefore, with considering the superiority of the 3-chain model (Hubert et al. 1943) in connecting the macroscopic mechanical behavior with the microstructure of VE material, the Abel fractional element is herein coupled into the framework of 3-chain model to describe the force-displacement relationship of a single chain in the 3-chain model, as:

$$F_{3ch} = \zeta (i\omega)^{\gamma} (r - r_0) = E_{3ch} (r - r_0) \tag{14}$$

where F_{3ch} is force at the end of molecular segment force in 3-chain model, and E_{3ch} is the equivalen stiffness of a single chain. The corresponding strain energy for a single chain w_v then is determined, as:

$$w_v = \frac{1}{2} E_{3ch} (r - r_0)^2 \tag{15}$$

According to the geometric characteristics of 3-chain model, the volume of cube represented by the 3-chain network is r_0^3. Based on Equation (15), the contribution of a single free chain per unit volume to the viscosity of VE material can be represented by the resulting Abel 3-chain model, and the viscous strain energy W_v is then formulated as:

$$W_v = \frac{N_2}{2r_0^3} \cdot \frac{1}{3} \sum_{j=1}^{3} \zeta (i\omega)^{\gamma} \left(r_j - r_0\right)^2 \tag{16}$$

where N_2 is the number of free chains per unit volume, r_j . Based on Equation (3)-(4), the viscous stress σ_v for characterizing the viscosity of VE material is then determined as:

$$\sigma_v = \frac{1}{3r_0} N_2 \zeta (i\omega)^{\gamma} \varepsilon \tag{17}$$

Consideration of the constraints from ambient molecular chains

Because of the constraint effect among the molecular chains, the macroscopic mechanical behavior of VE material is significantly strengthened. To describe the phenomenon associated with such constraint, the tube model (Doi et al. 1988) is introduced here to reflect the constraint strain energy function for VE material, which can be simplified as shown in Figure 4.

The constraint probability density of a single molecular chain in a tube under finite deformation can be expressed by (Miehe and Göktepe 2005):

$$P_v = P_{v0} \cdot exp\left[-\alpha \left(\frac{r_0}{R_{intial}}\right)^2 \nu\right] \tag{18}$$

where P_{v0} is the normalized parameter, R_{intial} is the tube diameter in the initial configuration, α is the material constant related to the crosssection of the tube, and ν is the shrinkage ratio of the tube's cross section. Based on Boltzmann's law, the relationship between the change of strain energy and its entropy is expressed as:

$$\Delta w = -T_0 \Delta s \tag{19}$$

According to Equation (18) and Equation (19)，the free energy constrained by a single molecular chain tube w_v can be obtained by

$$w_v = \alpha k T_0 \left(\frac{r_0}{R_{intial}}\right)^2 \nu + w_0 \tag{20}$$

where w_0 is a constant. Assuming that the unit vector of a single molecular chain is $\mathbf{M} = [\mathbf{e_1}, \mathbf{e_2}, \mathbf{e_3}]$, where $\mathbf{e_1}$, $\mathbf{e_2}$ and $\mathbf{e_3}$ are the coordinates of the molecular chain vector, the relationship between the constraint variables of the tube model ν and the macro elongation of the molecular chain λ can be described by the following equation based on Nanson formula (Miehe et al. 2004):

$$\nu = \mathbf{J}^{-1} \cdot (\mathbf{M}\mathbf{C}^{-1}\mathbf{M})^{1/2} \tag{21}$$

where C is the right Cauchy-Green deformation tensor. $\mathbf{J}^2 = 1$ under incompressible condition. Assuming $l = \alpha \left(\frac{r_0}{R_{intial}}\right)^2$, the reinforcement of the constraint from molecular chain network to the material mechanical property can be equivalently reflected by the constraint strain energy W_c, which is

$$W_c = NkT_0 l(\mathbf{I}_2)^{1/2} + W_0 \tag{22}$$

where W_0 is a constant, $N = N_1 + N_2$ is the total number of molecular chains per unit volume, $\mathbf{I}_2 = \lambda_1^2\lambda_2^2 + \lambda_2^2\lambda_3^2 + \lambda_3^2\lambda_1^2$ is the invariant of right Cauchy-Green strain tensor. As a result, constraint stress from the surrounding molecular chains σ_c is represented as:

$$\sigma_c = \frac{4\sqrt{3}}{3} NkT_0 l\varepsilon \tag{23}$$

Mathematical model of VE damper

According to the theoretical derivations in the aforementioned sections, it can be observed that the procedure of model establishment is a process of cross-scale characterizing the mechanical behavior of VE damper, which can be summarized as shown in Figure 5.

Substituting Equation (10), (17), and (23) into Equation (1) yields the shear dynamic modulus of the unfilled VE material $\bar{G}^*$, as:

$$\bar{G}^* = \frac{3\sqrt{3}\xi N_1}{4r_0} \frac{pq\omega^2 + q\omega i}{1 + p^2\omega^2} + (1-\xi)4N_1 kT_0 + \frac{N_2\zeta}{3r_0}(i\omega)^\gamma + \frac{4\sqrt{3}}{3} NkT_0 l \tag{24}$$

where the first and second parts of Equation (24) represent the influence of non-Gaussian and Gaussian statistics of molecular chains on the mechanical behaviors of VE damper, and another two parts reflect the chain viscosity and network structure constrain to a single chain.

However, the macroscopic mechanical performance of VE material is not only related to its internal molecular chain structure but also affected by the filling condition. The addition of fillers makes the molecular chains gather on the fillers and form a physically cross-linked structure, further constraining the deformation and movement of the molecular chains. Besides, due to the difference of stiffness between filler particles and the matrix rubber, fillers may amplify the deformation of the rubber matrix, introducing a significant discrepancy in the stiffness and energy dissipation capacity between the filler and the filler-free system. The actual filler-matrix structure of VE material can be seen in Figure 1. Generally, the enhancement of fillers can be considered by modifying the modulus of the unfilled matrix as:

$$G^* = \beta \bar{G}^* \tag{25}$$

where G^* is the modulus of the filled VE material, and β is the modulus amplification function, which can be determined by (Shaw and MacKnight 2018; Wang et al. 2015):

$$\beta = \begin{cases} 1 + 2.5\varphi + 14.1\varphi^2 & \varphi < 0.3 \\ [1/(1 - \varphi/\varphi_{max})]^{2.5\varphi_{max}} & \varphi > 0.3 \end{cases} \tag{26}$$

where φ is the volume fraction of the fillers, φ_{max} is the maximum volume fraction of the filler with the value of 0.637 in case of random filling.

Substituting $i^\gamma = \cos(\gamma\pi/2) + i\sin(\gamma\pi/2)$ into Equation (25), the energy-dissipation parameters of VE damper can be determined by separating the real part and the imaginary part of G^*, as:

$$G_1 = \frac{3\sqrt{3}N_1\beta\xi pq\omega^2}{4r_0(1 + p^2\omega^2)} + \frac{N_2\beta\zeta\,\omega^\gamma\cos(\gamma\pi/2)}{3r_0} + 4N_1\beta kT_0(1 - \xi) + \frac{4\sqrt{3}}{3}N\beta kT_0 l \tag{27}$$

$$G_2 = \frac{3\sqrt{3}N_1\beta\xi q\omega}{4r_0(1+p^2\omega^2)} + \frac{N_2\beta\zeta\omega^\gamma \sin(\gamma\pi/2)}{3r_0} \tag{28}$$

$$\eta = \frac{G_2}{G_1} \tag{29}$$

where G_1, G_2, and η are storage modulus, loss modulus, and loss factor for VE damper. With considering the effect of ambient temperature on the material dynamic property, the temperature-frequency equivalent principle (Kasai 2001; Li et al. 2021; Xu et al. 2011) is introduced to reflect the temperature sensitivity of VE materials, as.

$$\begin{cases} G_1(\omega, T) = G_1(\alpha_T\omega_r, T_r) \\ \eta(\omega, T) = \eta(\alpha_T\omega_r, T_r) \end{cases} \tag{30}$$

where $\alpha_T = 10^{-12(T-T_r)/[525+(T-T_r)]}$ is the temperature shift factor, ω_0 is the corresponding circular frequency, T and T_r are real-time ambient temperature and reference temperature, respectively.

Substituting Equation (30) into Equation (27)-(29), the microstructure-based equivalent visco-hyperelastic model for describing the mechanical properties of VE damper is finally completed, as:

$$G_1 = \frac{3\sqrt{3}N_1\beta\xi pq\alpha_T^2\omega^2}{4r_0(1+p^2\alpha_T^2\omega^2)} + \frac{N_2\beta\zeta\,\alpha_T^\gamma\omega^\gamma\cos(\gamma\pi/2)}{3r_0} + 4N_1\beta kT_0(1-\xi) + \frac{4\sqrt{3}}{3}N\beta kT_0 l \tag{31}$$

$$G_2 = \frac{3\sqrt{3}N_1\beta\xi q\alpha_T\omega}{4r_0(1+p^2\alpha_T^2\omega^2)} + \frac{N_2\beta\zeta\alpha_T^\gamma\omega^\gamma \sin(\gamma\pi/2)}{3r_0} \tag{32}$$

$$\eta = \frac{G_2}{G_1} \tag{33}$$

where Equations (31), (32), and (33) can explain the energy-dissipation mechanism of VE dampers from a microstructural level.

Dynamic property tests of VE dampers

Test protocols

To evaluate the prediction capacity and applicability of the proposed model, a series of experiments on the VE dampers at different temperatures and frequencies have been carried out. The experimental VE dampers were of classical sandwich configuration with two VE layers and three steel plate layers connected by vulcanization. The thickness of the VE layer of the tested VE damper is 10 mm with a shear area of 3000 mm^2. The volume fraction of the filler for the testing VE damping material is 0.2. A sinusoidal displacement loading protocol, $\varepsilon = \varepsilon_0 e^{i\omega t}$, was adopted in the testing process, where ε, ε_0, t are the actual strain, the applied strain amplitude, and time. Each loading condition consisted of 5 cycles, and the average of the middle three cycles is taken to represent the experimental result. The actual test setup is shown in Figure 6.

Considering the possible ambient temperature that may occur during the service process in practice, the test temperature range was controlled at 0 ~ 50 °C with a customized temperature-controlled chamber. In practice, seismic motion to which the structure is subjected to belongs to low-frequency load, so the loading frequency is set within 0~6 Hz. In addition, in order to avoid the influence of the VE nonlinearity of VE damper on its mechanical properties under large displacement (Li et al. 2021), which is not the focus of this study, the loading strain amplitude is kept within 50% in the test process. The experiment protocols are listed in Table 1. The whole experiments were divided into two groups, group 1 was employed for the latter model parameter identification, whereas group 2 was subsequently used for the assessment of the proposed model.

Test results and analysis

Figure 7 presents the measured hysteresis curves of VE dampers at different loading conditions. It can be observed that all the VE dampers exhibit plump hysteresis curves, indicating that their energy dissipation capacity is excellent. On the other hand, the variation of hysteresis curves under different

ambient temperatures, loading frequencies, and strain amplitudes are different. With the increase of loading frequency, the hysteresis curves become increasingly plump and tend to be flat with the increase of ambient temperature. With the strain amplitude experienced by VE dampers increasing, the plumpness of hysteresis curves keeps the visible increase. Similarly, from the macroscopic qualitative point of view, it can be seen from Figure 7 that the ambient temperature has the greatest influence on the area of the hysteresis curves, the strain amplitude contributes the second, and the frequency is relatively the smallest.

Figure 8 quantitatively presents the energy dissipation of a single hysteresis loop at different loading conditions. It can be concluded that the increase of loading frequency significantly promotes the energy-dissipation capacity of VE dampers, and the strain amplitude is positively correlated with the energy dissipation of VE dampers in approximately power-function form, whereas high temperature drastically reduces its energy dissipation capacity. Also, it can be observed that the energy-dissipation capacity of VE dampers shows a non-linear increase trend with the increase of frequency, and the increase rate at the low-frequency range is higher than that at the high-frequency range. For instance, when the loading frequency increases from 0.1 Hz to 2.0 Hz, the increment of energy consumption per cycle is 1.601 J, and this value changes to 0.330 J with the frequency increases from 4.0 Hz to 6.0 Hz. As for the ambient temperature, the reduction rate in the low-temperature range is also more pronounced than that in the high-temperature range. However, this rule does not apply to the strain amplitude, the energy dissipation of VE damper of a single cycle keeps a continuously increasing trend with the increase of strain amplitude.

The storage modulus G_1 and loss factor η are important parameters to represent the mechanical characteristics of VE dampers. The experimental results for these parameters are determined by the following equations:

$$G_1 = \frac{F_1 h_v}{n_v A_v u_0} \tag{34}$$

$$\eta = \frac{F_2}{F_1} \tag{35}$$

where F_1 and F_2 are the corresponding force at the maximum displacement u_0 and zero displacements respectively, n_v is the number of VE layers, A_v and h_v are the shear area and thickness of the VE layer. For the tested specimens, the corresponding parameters are calculated and shown in Table 2 and Figure 9.

Figure 9 shows the variation of the characteristic indicators, including G_1 and η, with ambient temperatures, loading frequencies, and strain amplitudes. It can be seen that with the increase of loading frequency, the storage modulus and loss factor of VE damper all exhibit an increasing tendency, and the change rate of these parameters in the lower-frequency range is remarkably higher than that in the high-frequency range. For example, when the frequency increases from 0.1 Hz to 2 Hz, the changes of G_1 and η are 0.257 MPa and 0.209, respectively, whereas these values become 0.031 MPa and 0.078 with frequency increasing from 4 Hz to 6 Hz. This indicates that the improvement in the energy consumption and stiffness caused by the increasing frequency tends to become stable with the increase of frequency under a high-frequency condition. This phenomenon may be explained by the fact that under high-frequency loading the cyclic period of the loading becomes much shorter than the material relaxation time, which is determined by the motion state of molecular chains inside material, rendering the material to be less frequency-sensitive. From the relationship between the characteristic parameters and the varying ambient temperature, it can also be seen that the degradation rates of these two

parameters are more significant in the low-temperature range than that in the high-temperature range, and this is can be contributed to the consolidation state of molecular chain and the difficulty of its corresponding motion at different temperature. As for the strain amplitude, the overall reduction tendency of G_1 and η are similar to that of temperature, which may be caused by the accumulated damage of the VE damper during the process of loading.

Validation and parameter analysis of the proposed model

Comparison with experimental data

The parameter identification process is to search a set of undetermined parameters to minimize the objective function Φ. Based on the test results in Section 3.2, the model parameters are identified by the genetic algorithm toolbox in MATLAB. Objective function Φ used in the fitting process is constructed as:

$$\Phi = \frac{\sum_{j=1}^{n_{test,1}}\left[G_{1,cal}^{j}(\omega,T,\varepsilon,\boldsymbol{\kappa}) - G_{1,test}^{j}\right]^2 + \sum_{j=1}^{n_{test,2}}\left[\eta_{cal}^{j}(\omega,T,\varepsilon,\boldsymbol{\kappa}) - \eta_{test}^{j}\right]^2}{n_{test,1} + n_{test,2}} \tag{36}$$

Where ω, T, ε, $G_{1,test}$, η_{test} are the test values of measured loading frequency, ambient temperature, strain amplitude, storage modulus, and loss factor, respectively. j represents the j th test value. $G_{1,cal}^{j}(\omega,T,\varepsilon,\kappa)$ and $\eta_{cal}^{j}(\omega,T,\varepsilon,\kappa)$ are the predicted values of the j th storage modulus and loss factor. $n_{test,1}$ and $n_{test,2}$ are the number of $G_{1,test}$ and η_{test}. $\boldsymbol{\kappa}$ is the undetermined parameter vector of the proposed model, which is

$$\boldsymbol{\kappa} = (N_1, N_2, p, q, \zeta, T_{\mathrm{r}}, \gamma, l, r_0, \varepsilon_{\mathrm{tr}}) \tag{37}$$

The model coefficients so identified for the test VE dampers, based on the tested data in experimental group 1, are listed in Table 3.

To illustrate the accuracy of the microstructure-based equivalent visco-hyperelastic constitutive model on describing the macroscopic mechanical behaviors of VE dampers, the proposed model with the above-identified parameters is employed to predict the experimental results of test group 2 in Table 1. The calculated results are listed in Table 4~Table 6, and Figure 10. As observed, almost all the absolute errors of predicted values for the storage modulus and loss factor are within the 20% tolerance given in this paper according to the literature (Li et al. 2021; Xu et al. 2016; Xu et al. 2019; Xu et al. 2019; Xu et al. 2013), from which the maximum calculated errors are generally within 20%. Therefore, it is suggested that a model be considered as producing has a good prediction accuracy when its numerical error is less than 20%. In fact, the averages prediction error of the proposed model in this paper are quite small, being 6.06% and 5.84% for G_1 and η, respectively. The maximum prediction errors for G_1 and η under different frequencies are just 8.49% and 12.61%, and change to 18.91% and 6.13% at different temperatures, while the maximum errors at different strain amplitudes are 15.58% and 12.17%, respectively. Thses results are markedly better than the maximum predicted errors of the proposed mathematical model in some previous studies (Xu et al. 2016; Xu et al. 2020; Xu et al. 2019).

Besides, to clarify the effectiveness of the minimization scheme on the parameter identification process, regression analysises are conducted based on the numerical results. The average residuals for G_1 and η are then calculated, which are only -0.001 and 0.002 and are close to zero. On the other hand, the goodness of fit is employed to measure the degree to which the predicted value fits the experimental results, and the corresponding determination coefficients for G_1 and η are computed up to 0.65 and 0.97, respectively, which further proofs the effectiveness of the model parameter determine stratage. It can also be seen that, in general, the predictive error of η is higher than that of G_1.This is because that G_1 is calculated directly, η is calculated indirectly, and the error in the calculation process will

gradually accumulate into the calculation results of η. Based on the numerical results, it can be concluded that the proposed model possesses a remarkable predictive accuracy and robustness in the description of storage modulus and loss factor for VE dampers under various loading frequencies, temperatures, and strain amplitudes.

In the sinusoidal shear deformation mode, the force-displacement curve of VE damper under various working conditions will exhibit as a standard ellipse, as shown in Figure 7. (Xu et al. 2016; Xu et al. 2020) present the force-displacement curve equation for VE dampers, which is

$$\left(\frac{\sigma - K_e\varepsilon}{\eta K_e \varepsilon_0}\right)^2 + \left(\frac{\varepsilon}{\varepsilon_0}\right)^2 = 1 \tag{38}$$

where $K_e = \frac{n_v G_1 A_v}{h_v}$ is the equivalent stiffness of the VE damper. Based on Equation (38) and the proposed model, the experimental hysteretic curves at different testing conditions can be calculated, as shown in Figure 11.

As observed, with varying loading frequencies, ambient temperatures and max strains, the experimental points basically fall on the numerical curves, indicating that the numerical hysteretic curve is generally in good agreement with the experimental results. On the other hand, considering that the hysteretic energy dissipation is an important indicator to describe the capacity of VE damper on mitigating the structural seismic response, the comparisons of energy dissipation per hysteresis loop between experimental and numerical results for the above numerical cases are conducted, and are listed in Table 7. It can be seen that almost all the calculation errors of the predicted values are no more than 14%, and the maximum prediction errors is only 13.72%, which can be concluded that the proposed mathematical model posesses significant accuracy and applicability in describing the hysteretic energy dissipation of VE dampers.

Also, it should be pointed out that the occurrence of some errors is inevitable and this can be attributed to the experimental error, discreteness of test data, and the simplifications made in the establishment of the proposed model. Although the complex microstructure and external factors that could affect the mechanical properties have been considered in this paper, other factors such as the specific distribution of fillers and cumulated damage in the loading process are still not accounted for. However, all the predicted errors are basically within an acceptable range, and the model proposed in this paper may be regarded as reasonably reflecting the mechanical behavior of VE dampers in applications.

Analysis of the microstructure-based parameters

As can be seen, microstructure parameters in this model can relate the macro mechanical properties of VE damper to the microstructure of VE material from micro-perspectives. Among them, the number of molecular chains, the initial end-to-end distance of the molecular chain, and the constrain coefficient are three essential microscopic parameters for the proposed model to characterize the mechanical behavior of VE damper from a cross-scale perspective. To further study the influence of material microstructure on its macroscopic performance, these three microscopic model parameters are selected, and then normalized with the above-identified parameters to make the same numerical simulation on the experiments with other parameters keeping constant. Considering the effects of loading frequency, ambient temperature, and strain amplitude on the mechanical properties of VE dampers have been experimentally investigated in Section 3.2, in this section, the characteristic parameters of VE damper under different frequencies are predicted by the proposed model, and the influence of microstructure-based parameters on the prediction results is then analyzed quantitatively. The calculation results under are graphed in Figure 12 ~ Figure 14.

Figure 12(a) shows that the storage modulus increases with the increase of N_2/N_1, and the increase rate at high frequency is significantly higher than that at low frequency. Generally speaking, the increase of the number of free chains can lead to the reduction of the elastic chain by assuming that the total number of molecular chains per unit volume is constant. In fact, the elastic chains and free chains contribute to both elasticity and viscosity of VE material as mentioned earlier. When the increase of the free chain to the material elasticity is enough to compensate for the decrease of the material elasticity caused by the decrease of the elastic chain, the VE material could show the trend of increasing the storage modulus instead. Besides, due to the high entropy elasticity of the elastic network chain, the natural vibration frequency of a single elastic molecular chain is high, leading it is more sensitive to high frequency. So that the vibration of a single molecular chain at high frequency is fierce than that at low frequency, the VE damper hence shows the phenomenon of modulus enhanced. Figure 12(b) demonstrates that the loss factor increases with the increase of N_2/N_1, the reason may be that the energy consumption of the VE material is mainly due to the friction between the free molecular chains itself and with the elastic chain, and the increase of the number of free chains then cause the increase of the loss modulus of VE dampers.

It can be observed from Figure 13 that, both the storage modulus and loss factor increase with the decrease of r_0. This is because that the smaller r_0 is, the higher the curl degree of molecular chain is. Thus, the molecular chain possesses higher configuration entropy and friction with the surrounding chains, leading to the macroscopic performance of strong elasticity and viscosity. Besides, the promotion rate of the material modulus and loss factor show the trend of degradation with the increase r_0. This phenomenon may be explained that the entropy elasticity can be very low due to the low-level curl degree of molecular chain, and the molecular chain in the matrix is in a highly loose free state,

similar to a dilute polymer solution, resulting in that the material is not sensitive to the change of r_0. On the other hand, Figure 13 also demonstrates that increase rates of the storage modulus and loss factor at high frequency is more significant than that at low frequency at different r_0, this may because that the vibration period of molecular chain is close to the high frequency in the calculations so that the VE damper shows higher stiffness and dissipation capacity.

As seen from Figure 14, with the increase of l, the storage modulus of VE damper remarkablely gets enhanced with its loss factor slightly decreasing. The reason may be that the elasticity provided by the elastic network chain mainly comes from the entropy elasticity of a single molecular chain, which is not only related to its curl degree but also related to its surrounding network constraints. Raw rubber is usually vulcanized and crosslinked in engineering so that more crosslinking points are formed between the molecular chains in the material, which increases the mutual constraints between the molecular chains, and finally improves the storage modulus of VE material. However, higher curl and crosslink of molecular chain can obtain higher material strength, but it will sacrifice the dissipation capacity of the VE material. For a given material, the more elastic chains formed, the fewer free chains left, and the weaker the energy dissipation capacity of the VE damper, which is not conducive to the energy dissipation of the actual structure.

Conclusions

In this paper, a microstructure-based equivalent visco-hyperelastic model is presented. A series of dynamic property tests on VE dampers are carried out. The accuracy and applicability of the proposed model are verified by the test data, sensitivity analysis on the microstructure parameters is conducted. The following conclusions may be drawn:

(1) The comparative results demonstrate that the model is capable of reflecting the energy dissipation and stiffness characteristics of VE dampers under varying loading frequency, ambient temperature, and strain amplitude. The parameters of the proposed model have clear physical meanings, allowing a rubust representation of the relationship between the macroscopic mechanical characteristics of VE dampers and the complicated microstructure of VE materials.

(2) The initial configuration, composition, and network topology of molecular chain have a significant effect on the macroscopic mechanical behaviors of VE dampers. For a given material, with the increase of the ratio of the number of free chains to elastic network chains, the storage modulus and the loss modulus simultaneously increases in the test frequency ranges. With the decrease of the initial end-to-end distance of molecular chain, both the storage modulus and loss modulus significantly increase. With the increase of the constraint between molecular chains, the storage modulus of VE dampers gets enhanced, whereas its loss factors observably decrease.

(3) VE dampers possess an excellent energy dissipation capability, which is remarkably affected by the varying temperature, frequency, and strain amplitude. Increasing loading frequency significantly promotes the energy dissipation capacity of VE dampers, whereas high temperature causes drastic degradation in its energy dissipation capacity. The change rates of the characteristic parameters tend to be more pronounced in the lower ranges of frequency and temperature than that in the higher ranges.

(4) It should be pointed out that, although the proposed model has considered the complex structural characteristics of the macromolecular chain and other external factors that may affect the macroscopic mechanical properties of VE dampers, several simplifications have also been made and this tends to lead to increased prediction errors in some situations. In future studies, other pertinent factors, such as

the internal damage of materials, the Payne effect, and the Mullins effect, should be examined and be appropriately included in the prediction model.

Data availability statement

All data, models, and code generated or used during the study appear in the submitted article.

Acknowledgments

The authors acknowledge financial supports for this research from National Key Research and Development Plans with Grant No. 2019YFE0121900, Program of Chang Jiang Scholars of Ministry of Education, the Tencent Foundation through the XPLORER PRIZE.

References

Boccaccio, A., Lamberti, L., Papi, M., Spirito, M. D., and Pappalettere, C. (2015). "A hybrid characterization framework to determine the visco-hyperelastic properties of a porcine zona pellucida." Interface Focus, 4(2), 86-108.

Boyce, M. C., and Arruda, E. M. (2000). "Constitutive models of rubber elasticity: a review." Rubber chemistry and technology, 73(3), 504-523.

Chang, K. C., and Lin, Y. Y. (2004). "Seismic response of full-scale structure with added viscoelastic dampers." *Journal of Structural Engineering*, 130(4), 600-608.

Chang, K. C., Soong, T. T., Oh, S. T., and Lai, M. L. (1992). "Effect of Ambient Temperature on Viscoelastically damped structure." *Journal of Structural Engineering*, 118(7), 1955-1973.

Doi, M., Edwards, S. F., and Edwards, S. F. (1988). *The theory of polymer dynamics*, oxford university press.

Dong, Y. R., Xu, Z. D., Li, Q. Q., Zhu, C., and He, Z. H. (2020). "Design parameters and material‐scale damage evolution of seismic upgraded RC frames by viscoelastic haunch bracing‐dampers." *Earthquake Engineering and Structural Dynamics*.

Elías-Zúñiga, A., and Beatty, M. F. (2002). "Constitutive equations for amended non-Gaussian network models of rubber elasticity." *International journal of engineering science*, 40(20), 2265-2294.

Hubert, M., James, E., Daniel, and Guth (1943). "Theory of the Elastic Properties of Rubber." *Journal of Chemical Physics*, 11.

Kasai, K. (2001). "Constitutive rule for viscoelastic materials considering temperature, frequency, and strain sensitivities." *Journal of Structural and Construction Engineering*, 543, 77-86.

Kroon, M. (2011). "An 8-chain Model for Rubber-like Materials Accounting for Non-affine Chain Deformations and Topological Constraints." *Journal of Elasticity*, 102(2), 99-116.

Lewandowski, R., and Pawlak, Z. (2011). "Dynamic analysis of frames with viscoelastic dampers modelled by rheological models with fractionalderivatives." *Journal of Sound and Vibration*, 330(5), 923-936.

Lewandowski, R., and Przychodzki, M. (2018). "Approximate method for temperature-dependent characteristics of structures with viscoelastic dampers." *Archive of Applied Mechanics*, 88(10), 1695-1711.

Li, Q. Q., Xu, Z. D., Dong, Y. R., He, Z. H., Zhu, C., and Lu, Y. (2021). "Effects of mechanical nonlinearity of viscoelastic dampers on the seismic performance of viscoelasticlly damped structures." *Soil Dynamics and Earthquake Engineering*, 150, 106936.

Li, Y., Tang, S., Abberton, B. C., Kröger, M., Burkhart, C., Jiang, B., Papakonstantopoulos, G. J., Poldneff, M., and Liu, W. K. (2012). "A predictive multiscale computational framework for viscoelastic properties of linear polymers." *Polymer*, 53(25), 5935-5952.

Lim, G. T. (2005). "Scratch behavior of polymers." Texas A&M University.

Marckmann, G., Verron, E., Gornet, L., Chagnon, G., Charrier, P., and Fort, P. (2002). "A theory of network alteration for the Mullins effect." *Journal of the Mechanics and Physics of Solids*, 50(9), 2011-2028.

Marrucci, G. (1988). "Fast flows of concentrated polymers: predictions of the tube model on chain stretching." *Gazz. Chim. Itali.*, 118, 179-185.

Miehe, C., and Göktepe, S. (2005). "A micro–macro approach to rubber-like materials. Part II: The micro-sphere model of finite rubber viscoelasticity." *Journal of the Mechanics and Physics of Solids*, 53(10), 2231-2258.

Miehe, C., Göktepe, S., and Lulei, F. (2004). "A micro-macro approach to rubber-like materials—part I: the non-affine micro-sphere model of rubber elasticity." *Journal of the Mechanics and Physics of Solids*, 52(11), 2617-2660.

Min, K. W., Kim, J., and Lee, S. H. (2004). "Vibration tests of 5-storey steel frame with viscoelastic dampers." *Engineering Structures*, 26(6), 831-839.

Shaw, M. T., and MacKnight, W. J. (2018). *Introduction to polymer viscoelasticity*, John Wiley & Sons.

Shim, V. P. W., Yang, L. M., Lim, C. T., and Law, P. H. (2010). "A visco-hyperelastic constitutive model to characterize both tensile and compressive behavior of rubber." *Journal of Applied Polymer Science*, 92(1), 523-531.

Tang, Shan, Greene, S., Liu, and Kam, W. (2012). "Two-scale mechanism-based theory of nonlinear viscoelasticity." *Journal of the Mechanics and Physics of Solids*, 60(2), 199-226.

Tomita, Y., Lu, W., Naito, M., and Furutani, Y. (2006). "Numerical evaluation of micro-to macroscopic mechanical behavior of carbon-black-filled rubber." *International Journal of Mechanical Sciences*, 48(2), 108-116.

Treloar, L. R. G. (1946). "The elasticity of a network of long-chain molecules. I." *Trans Faraday Soc*, 42.

Treloar, L. R. G., and Riding, G. (1979). "A Non-Gaussian Theory for Rubber in Biaxial Strain. II. Optical Properties." *Proceedings of the Royal Society A*, 369(1737), 281-293.

Wang, J., Jia, H., Ding, L., Xiong, X., and Gong, X. (2015). "The mechanism of carbon–silica dual phase filler modified by ionic liquid and its reinforcing on natural rubber." *Polymer Composites*, 36(9), 1721-1730.

Wu, P., and Van Der Giessen, E. (1993). "On improved network models for rubber elasticity and their applications to orientation hardening in glassy polymers." *Journal of the Mechanics and Physics of Solids*, 41(3), 427-456.

Xu, C., Xu, Z. D., Ge, T., and Liao, Y.-X. (2016). "Modeling and experimentation of a viscoelastic microvibration damper based on a chain network model." *Journal of Mechanics of Materials and Structures*, 11(4), 413-432.

Xu, C., Xu, Z. D., Teng., G., and X., L. Y. (2016). "Experimental and Numerical Study on Dynamic Properties of Viscoelastic Microvibration Damper Considering Temperature and Frequency Effects." *Journal of Computational and Nonlinear Dynamics*.

Xu, Y., Xu, Z. D., Guo, Y. Q., Dong, Y., Ge, T., and Xu, C. (2019). "Tests and Modeling of Viscoelastic Damper Considering Microstructures and Displacement Amplitude Influence." *Journal of Engineering Mechanics*, 145(12), 04019108.

Xu, Y., Xu, Z. D., Guo, Y. Q., Ge, T., Xu, C., and Huang, X. (2019). "Theoretical and Experimental Study of Viscoelastic Damper Based on Fractional Derivative Approach and Micromolecular Structures." *Journal of Vibration and Acoustics*, 141(3), 031010.

Xu, Z. D., Ge, T., and Liu, J. (2020). "Experimental and Theoretical Study of High-Energy Dissipation-Viscoelastic Dampers Based on Acrylate-Rubber Matrix." *Journal of Engineering Mechanics*, 146(6), 04020057.

Xu, Z. D., Ge, T., and Miao, A. (2019). "Experimental and theoretical study on a novel multi-dimensional vibration isolation and mitigation device for large-scale pipeline structure." *Mechanical Systems and Signal Processing*, 129, 546-567.

Xu, Z. D., Wang, D. X., and Shi, C. F. (2011). "Model, tests and application design for viscoelastic dampers." *Journal of Vibration and Control*, 17(9), 1359-1370.

Xu, Z. D., Xu, C., and Hu, J. (2013). "Equivalent fractional Kelvin model and experimental study on viscoelastic damper." *Journal of Vibration and Control*, 21(13), 2536-2552.

Yang, L. M., Shim, V. P. W., and Lim, C. T. (2000). "A visco-hyperelastic approach to modelling the constitutive behaviour of rubber." *International Journal of Impact Engineering*, 24(6/7), 545-560.

Zhou, X. Q., Yu, D. Y., Shao, X. Y., Zhang, S. Q., and Wang, S. (2016). "Research and applications of viscoelastic vibration damping materials: A review." *Composite Structures*, 136, 460-480.

List of Table Captions:

Table 1 Experiment protocols

Table 2 Characteristic parameters at different loading conditions

Table 3 Model parameters

Table 4 The experimental and numerical result comparisons for different frequencies when $max\ \ strain = 20\%$ and $T = 15^{o}\mathrm{C}$

Table 5 The experimental and numerical result comparisons for different temperatures when $max\ \ strain = 20\%$ and $\omega = 2.0\mathrm{Hz}$

Table 6 The experimental and numerical result comparisons for different max strains when $\omega = 2.0\mathrm{Hz}$ and $T = 15^{o}\mathrm{C}$

Table 7 Comparison of energy dissipation per hysteresis loop

Tables

Table 1 Experiment protocols

Test group	Temperature (°C)	Frequency (Hz)	Strain amplitude
	15	0.3, 1.0, 2.0, 3.0, 4.0, 6.0	20%
1	0, 10, 20, 30, 40	2.0	20%
	15	2.0	10%, 20%, 30%, 40%
	15	0.1, 0.5, 1.5, 2.5, 3.5,5.0	20%
2	5, 15, 25, 35, 45	2.0	20%
	15	2.0	5%, 15%, 25%, 35%

Table 2 Characteristic parameters at different loading conditions

ω(Hz)	0.1	0.3	0.5	1	1.5	2	2.5	3	3.5	4	5	6
G_1(MPa)	0.701	0.802	0.824	0.876	0.923	0.958	0.972	1.015	0.99	1.021	1.037	1.052
η	0.101	0.122	0.164	0.250	0.284	0.310	0.329	0.354	0.387	0.401	0.452	0.479
T (°C)	0	5	10	15	20	25	30	35	40	45	/	/
G_1(MPa)	1.56	1.01	1.076	0.958	0.872	0.817	0.779	0.755	0.733	0.688	/	/
η	0.856	0.429	0.388	0.310	0.235	0.201	0.160	0.156	0.136	0.129	/	/
Max strain	5%	10%	15%	20%	25%	30%	35%	40%	/	/	/	/
G_1(MPa)	1.056	0.997	0.974	0.958	0.927	0.904	0.882	0.846	/	/	/	/
η	0.353	0.336	0.318	0.310	0.307	0.303	0.291	0.279	/	/	/	/

Table 3 Model parameters

	Model parameter
The proposed model	$N_1 = 3.21 \times 10^{21},\ N_2 = 1.32 \times 10^{20},\ p = 5.56, q = 0.88,\ \zeta = 0.99,$ $T_r = 29.0,\ \gamma = 0.70,\ l = 1.24 \times 10^{4},\ r_0 = 8.07 \times 10^{12},\ \varepsilon_{tr} = 0.01$

Table 4 The experimental and numerical result comparisons for different frequencies when $max\ strain = 20\%$ and $T = 15^{o}C$

ω(Hz)	G_1(MPa)			η		
	Experimental data	Numerical results	Calculation error	Experimental data	Numerical results	Calculation error
0.1	0.701	0.761	8.49%	0.101	0.094	7.31%
0.5	0.824	0.826	0.18%	0.161	0.141	12.61%
1.5	0.923	0.889	3.72%	0.284	0.257	9.49%
2.5	0.972	0.938	3.51%	0.329	0.344	4.55%
3.5	0.990	0.981	0.88%	0.387	0.415	7.18%
5	1.037	1.040	0.29%	0.452	0.501	10.92%

Table 5 The experimental and numerical result comparisons for different temperatures when $max\ strain = 20\%$ and $\omega = 2.0Hz$

T (°C)	G_1(MPa)			η		
	Experimental data	Numerical results	Calculation error	Experimental data	Numerical results	Calculation error
5	1.010	0.982	2.74%	0.429	0.416	2.95%
15	0.958	0.914	4.57%	0.310	0.303	2.37%
25	0.817	0.870	6.45%	0.175	0.182	3.77%
35	0.755	0.840	11.21%	0.156	0.165	6.13%
45	0.688	0.818	18.91%	0.129	0.129	0.55%

Table 6 The experimental and numerical result comparisons for different max strains when $\omega = 2.0Hz$ and $T = 15^{o}C$

Max strain	G_1(MPa)			η		
	Experimental data	Numerical results	Calculation error	Experimental data	Numerical results	Calculation error
5%	1.056	0.892	15.58%	0.353	0.310	12.17%
15%	0.974	0.906	6.99%	0.318	0.305	4.03%
25%	0.927	0.923	0.41%	0.307	0.300	2.09%
35%	0.882	0.944	6.98%	0.291	0.295	1.45%

Table 7 Comparison of energy dissipation per hysteresis loop

Numerical cases	Energy dissipation per hysteresis loop (J)		
	Experimental results	Numerical results	Calculation error
(a)	1.373	1.361	0.87%
(b)	3.260	3.303	1.31%
(c)	2.467	2.128	13.72%
(d)	0.876	0.972	10.90%
(e)	1.456	1.273	12.52%
(f)	6.474	6.639	2.55%

Figure Captions:

Figure 1 Microstructure of VE material: (a) Actual micromorphological structures; (b) Simplified molecular chain network.

Figure 2 Evolution of statistical distribution for molecular chains

Figure 3 Different forms of transition equation: (a) Lim 2005; (b) the present paper; (c) Elías-Zúñiga and Beatty 2002

Figure 4 Tube model for describeing the constraints between molecular chains: (a) Initial configuration; (b) Immediate configuration after tension

Figure 5 Procedure of model establishment: Microscale: (a) Gaussian statistical model, (b) 8-chain statistical model, (c) 3-chain statistical model; Macroscale: (d) Maxwell element, (e) Abel fractional element

Figure 6 The actual testing status

Figure 7 Hysteresis curves of VE dampers at different frequencies, different temperatures and different Max strains: (a), (c), (e) group 1; (b), (d), (f) group 2.

Figure 8 Energy dissipation per hysteresis loop at different loading conditions

Figure 9 G_1 and η at different loading conditions

Figure 10 Experimental prediction of the proposed model at different conditions

Figure 11 Comparison of hysteretic curves between experimental and numerical results at different loading conditions; (a) and (b) $\mathrm{Max\ strains} = 20\%$, $\mathrm{T} = 15^{\mathrm{o}}\mathrm{C}$; (c) and (d) $\mathrm{Max\ strains} = 20\%$, $\omega = 2\mathrm{Hz}$; (e) and (f) $\mathrm{T} = 15^{\mathrm{o}}\mathrm{C}$, $\omega = 2\mathrm{Hz}$.

Figure 12 Influence of ratio of N_2/N_1

Figure 13 Influence of model parameter r_0

Figure 14 Influence of model parameter l

Figures

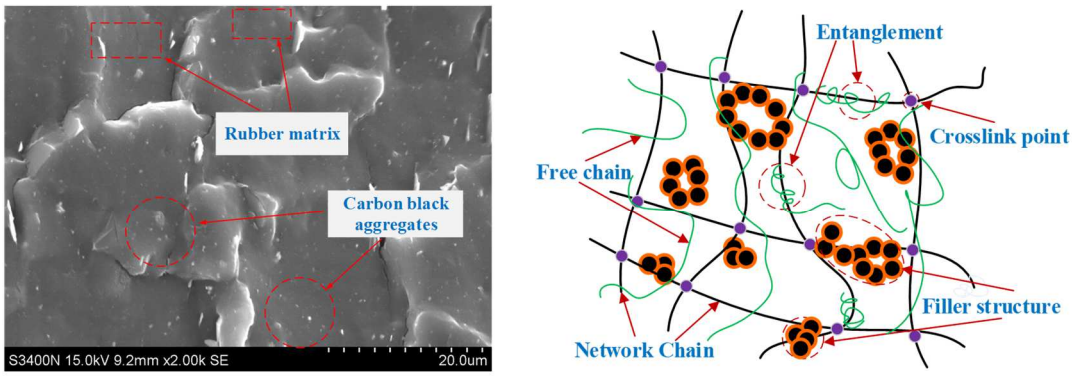

(a) Actual Micromorphology (b) Idealized Molecular Structure

Figure 1 Microstructure of VE material: (a) Actual micromorphological structures; (b) Simplified molecular chain network.

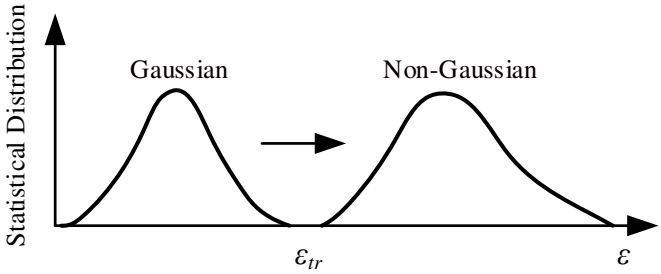

Figure 2 Evolution of statistical distribution for molecular chains

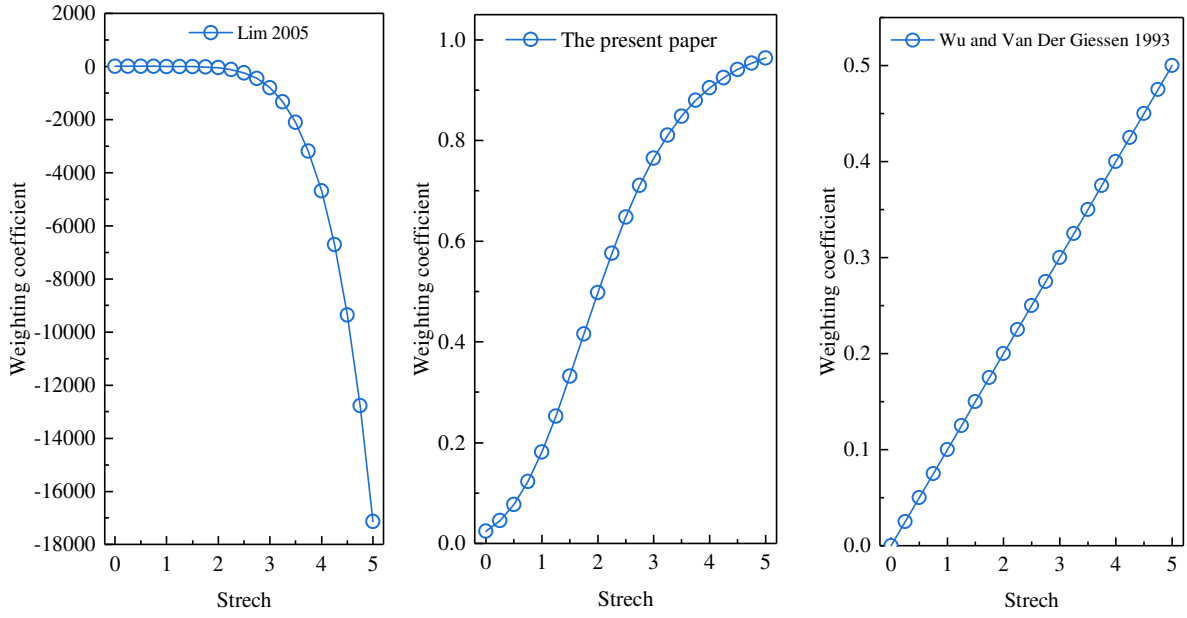

(a) **(b)** **(c)**

Figure 3 Different forms of transition equation: (a) Lim 2005; (b) the present paper; (c) Elías-Zúñiga and Beatty 2002

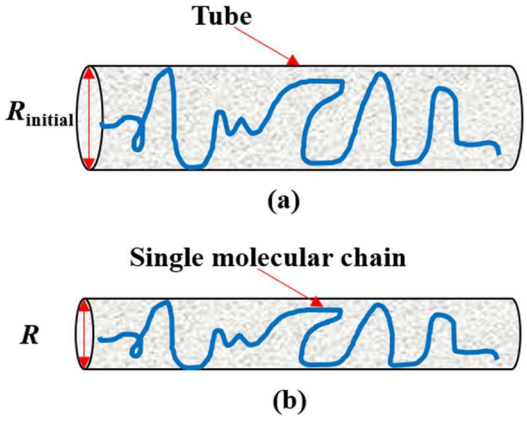

Figure 4 Tube model for describeing the constraints between molecular chains: (a) Initial configuration; (b) Immediate configuration after tension

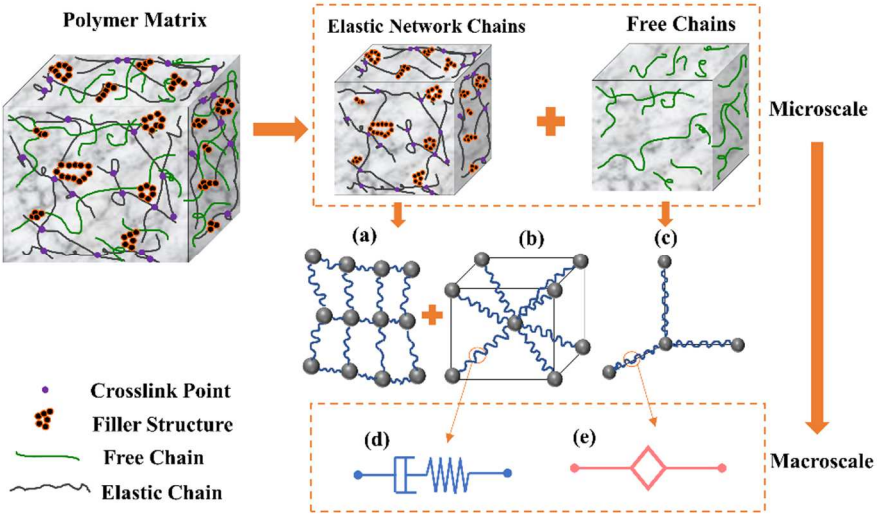

Figure 5 Procedure of model establishment: Microscale: (a) Gaussian statistical model, (b) 8-chain statistical model, (c) 3-chain statistical model; Macroscale: (d) Maxwell element, (e) Abel fractional element

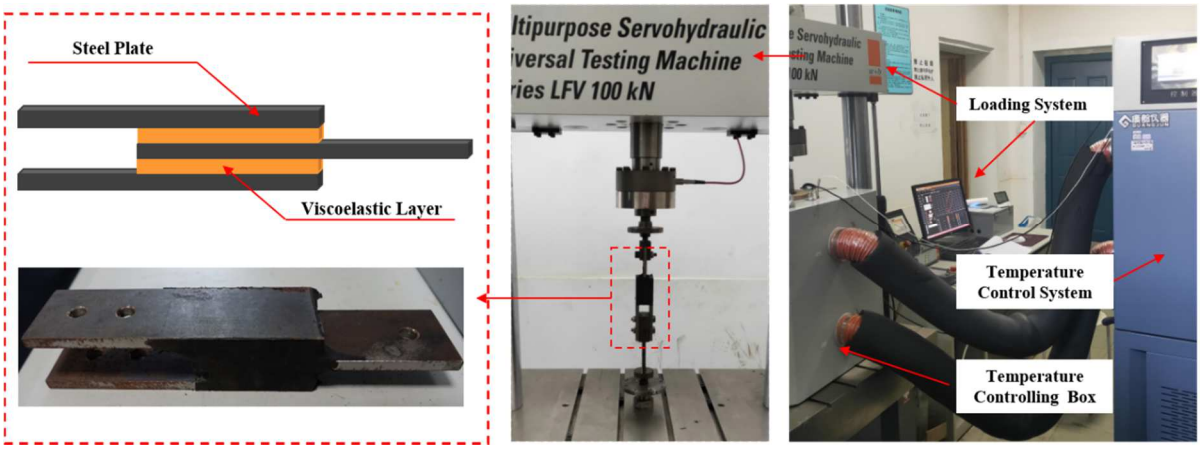

Figure 6 The actual testing status

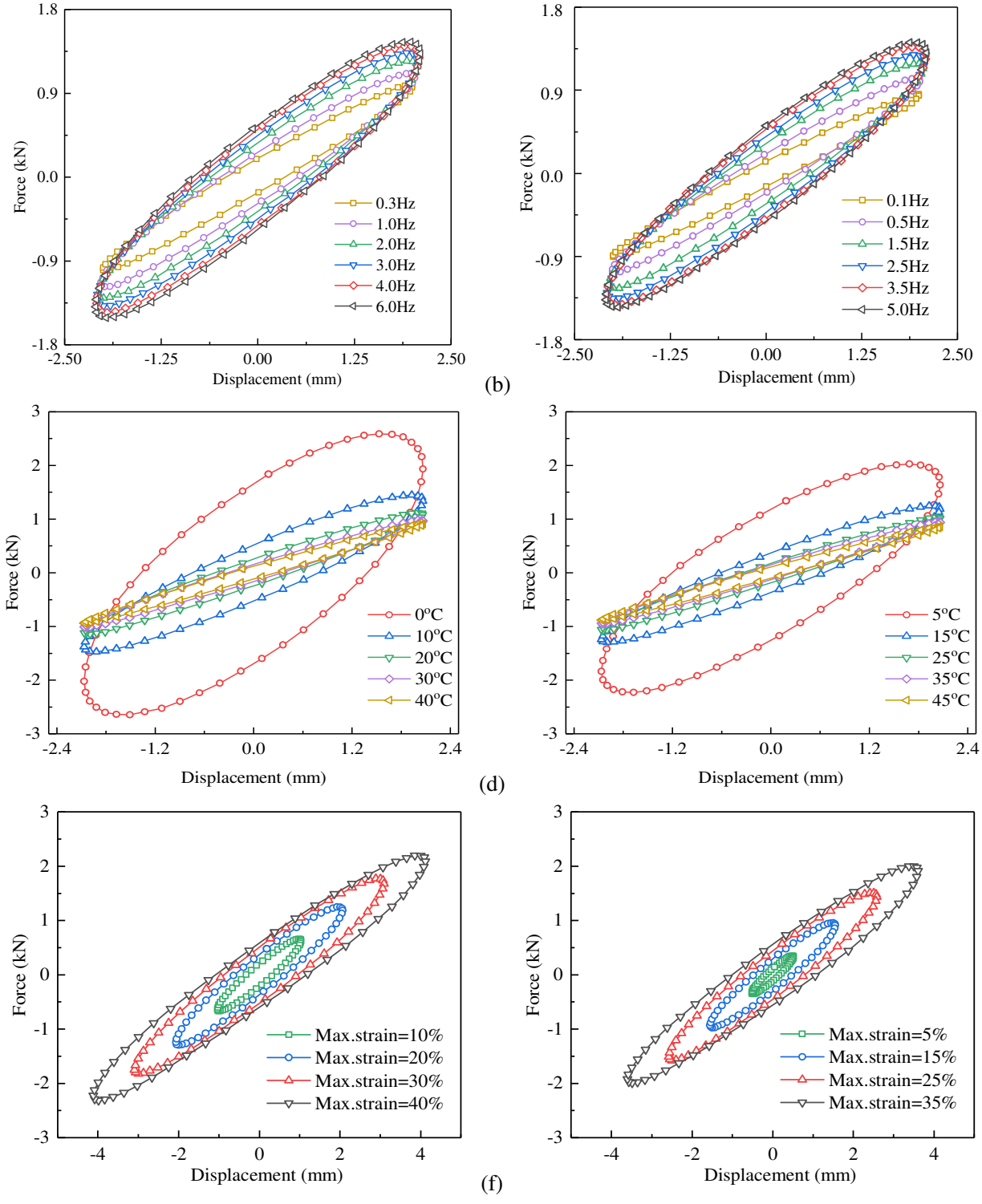

Figure 7 Hysteresis curves of VE dampers at different frequencies, different temperatures and different Max strains: (a), (c), (e) group 1; (b), (d), (f) group 2.

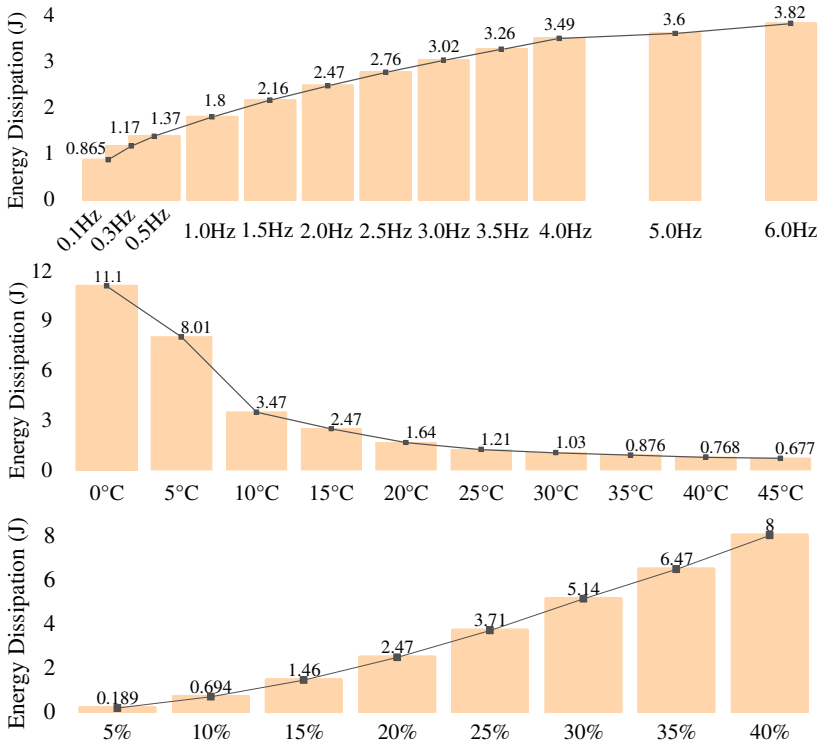

Figure 8 Energy dissipation per hysteresis loop at different loading conditions

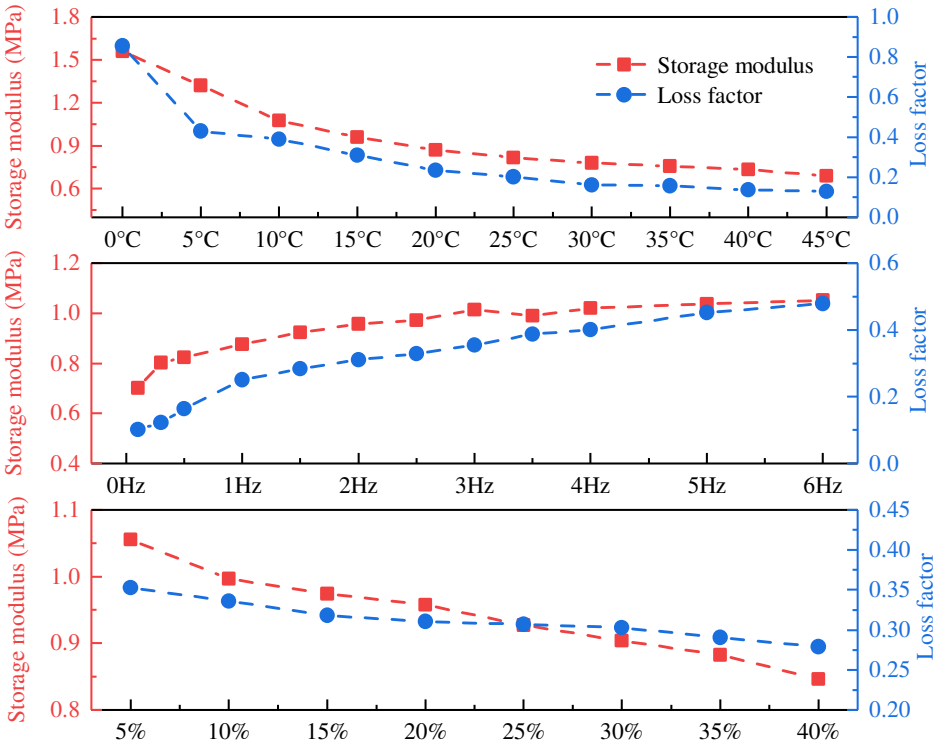

Figure 9 G_1 and η at different loading conditions

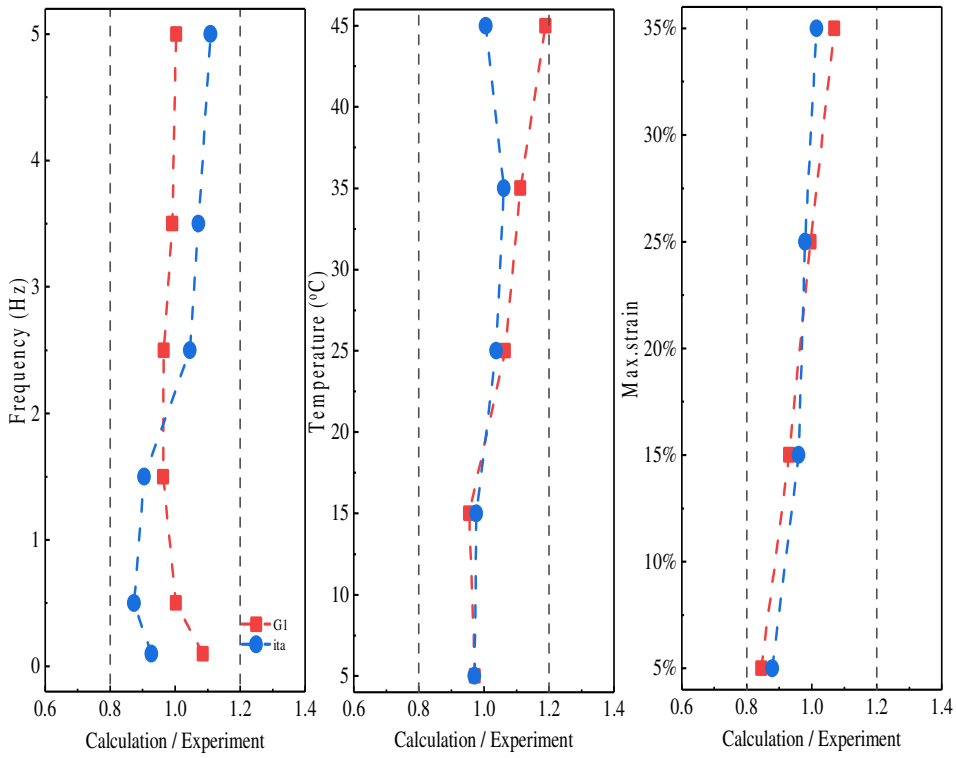

Figure 10 Experimental prediction of the proposed model at different conditions

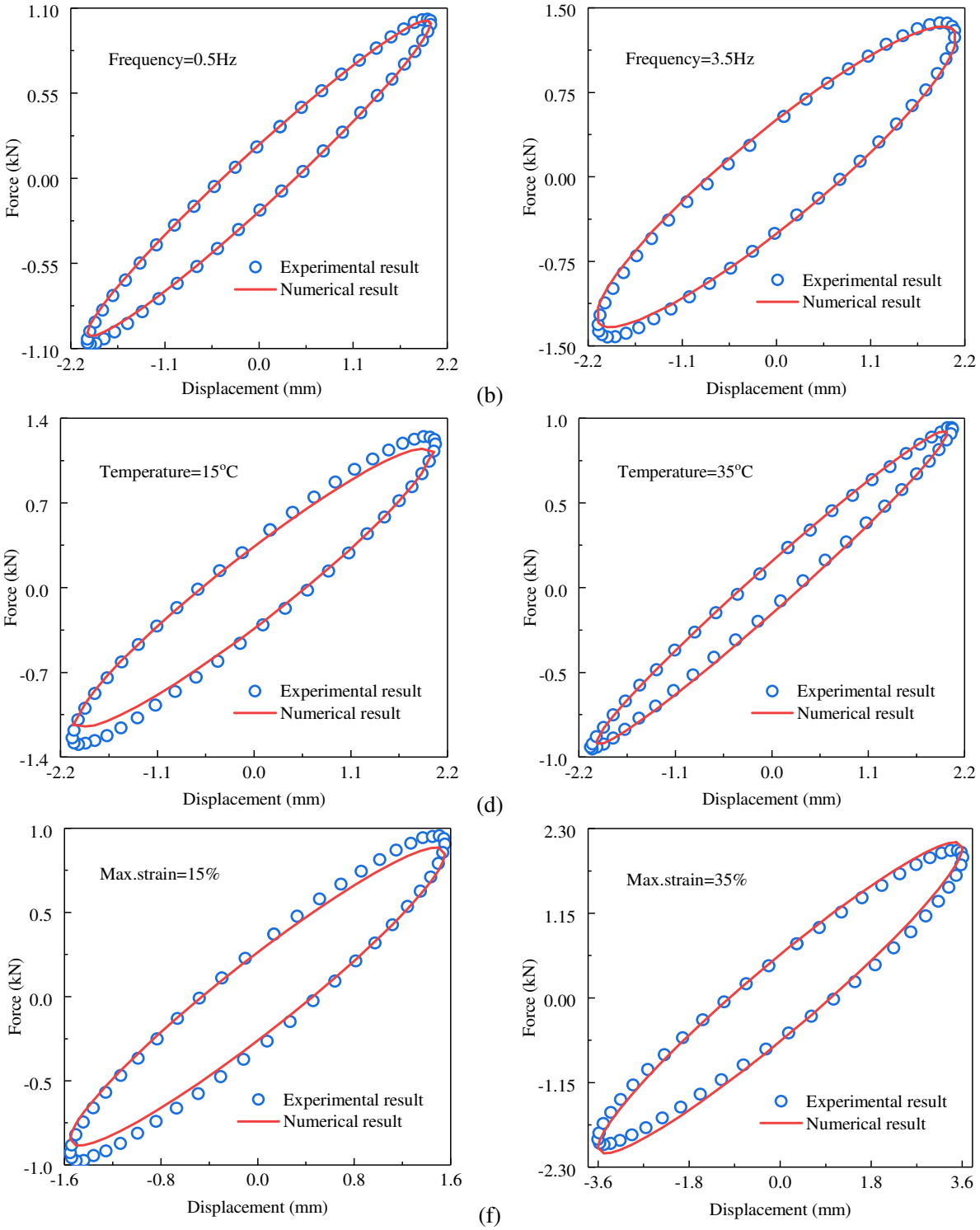

Figure 11 Comparison of hysteretic curves between experimental and numerical results at different loading conditions; (a) and (b) Max strains = 20%, T = 15°C; (c) and (d) Max strains = 20%, ω = 2Hz; (e) and (f) T = 15°C, ω = 2Hz.

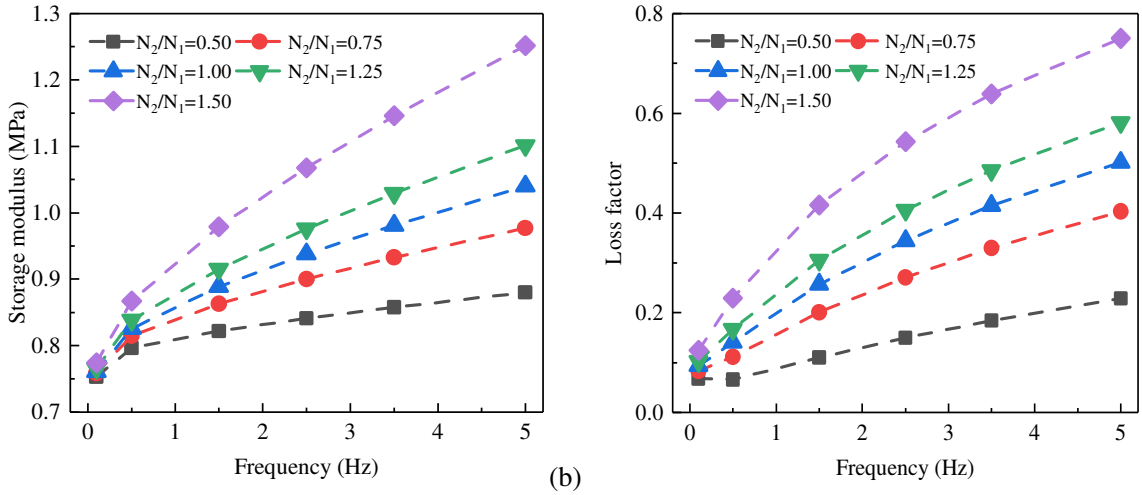

Figure 12 Influence of ratio of N_2/N_1; (a) G_1; (b) η.

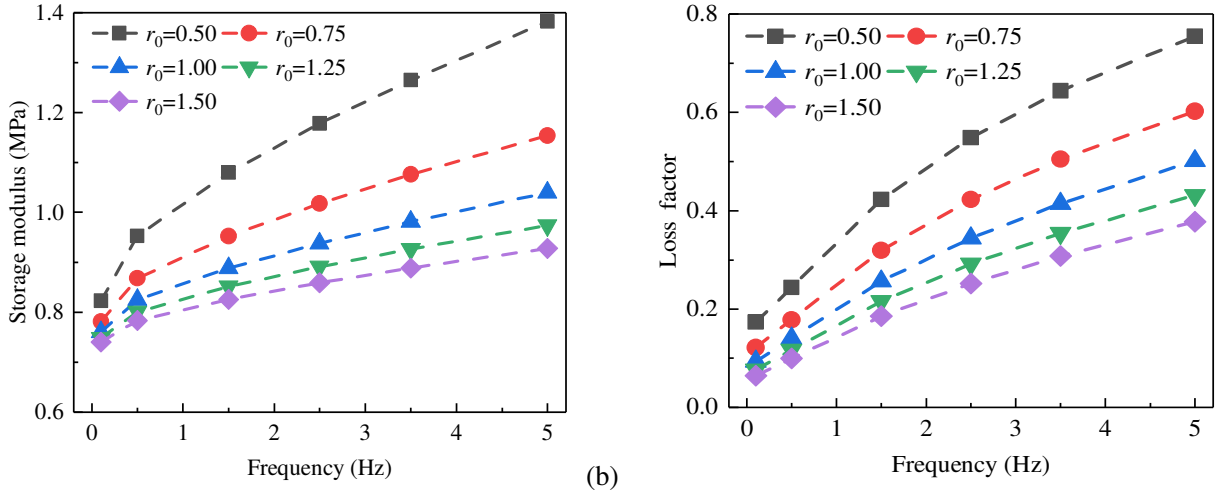

Figure 13 Influence of model parameter r_0; (a) G_1; (b) η.

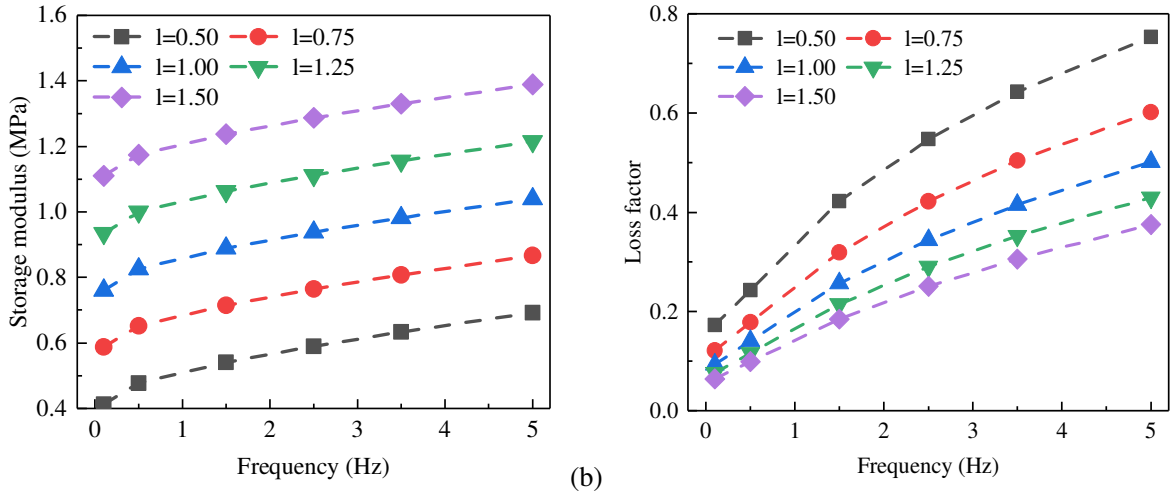

Figure 14 Influence of model parameter l; (a) G_1; (b) η.